Transport Barrier inside the Reversal Surface in the Chaotic Regime of the Reversed-Field Pinch

G. Spizzo,[1] S. Cappello,[1] A. Cravotta,[1] D. F. Escande,[1,2] I. Predebon,[1] L. Marrelli,[1] P. Martin,[1] and R. B. White[3]

[1]*Consorzio RFX, Euratom-ENEA Association, Corso Stati Uniti, 4 35127 Padova, Italy*

[2]*UMR 6633, CNRS-Université de Provence, F-13397 Marseille cedex 20, France*

[3]*Plasma Physics Laboratory, Princeton University, P.O. Box 451, Princeton, New Jersey 08543, USA*

(Received 11 March 2005; published 17 January 2006)

Magnetic field lines and the corresponding particle orbits are computed for a typical chaotic magnetic field provided by a magnetohydrodynamics numerical simulation of the reversed-field pinch. The $m = 1$ modes are phase locked and produce a toroidally localized bulging of the plasma which increases particle transport. The $m = 0$ and $m = 1$ modes produce magnetic chaos implying poor confinement. However, they also allow for the formation of magnetic islands which induce transport barriers inside the reversal surface.

DOI: 10.1103/PhysRevLett.96.025001 PACS numbers: 52.25.Fi, 45.20.Jj, 52.55.Hc, 52.65.Cc

The reversed-field pinch (RFP) is a magnetic configuration for plasma confinement where the toroidal field reverses slightly at the edge. Experiments and viscoresistive MHD simulations of the RFP reveal that this configuration may exist in a turbulent multiple helicity (MH) state. Strong temperature and density gradients are located at the reversal [1–4], but their origin is still under debate. This Letter aims to show that they are due to the presence of magnetic islands in the reversal region. The existence of such islands is indicated by several experimental measurements: total radiation and soft x-ray tomography [5,6], spectroscopy [7]. These measurements are consistent with the reconstruction of the last closed flux surface from edge magnetic fluctuation spectra [8].

On the basis of field line tracing applied to MHD simulations and of analytical Hamiltonian calculations, this Letter shows that the modes with poloidal number $m = 0$ and $m = 1$ have two opposite effects on particle confinement. The dominant one is negative: the modes produce magnetic chaos in the $q > 0$ region [3,9] which implies poor confinement. Furthermore, if $m = 1$ modes are phase locked, they also produce a toroidally localized bulging of the magnetic field lines and of the chaotic sea which increases transport as observed in experiments [10]. However, there is a secondary effect of $m = 0$ and $m = 1$ modes that mitigates their negative action on confinement: they allow for the formation of magnetic islands which induce a transport barrier inside the reversal radius.

The numerical part of this work is performed in two steps. First the 3D MHD nonlinear, viscoresistive cylindrical code SPECYL [11] computes the typical magnetic field of a MH state ($S = 3 \times 10^4$ and $\Theta = \frac{B_\theta(a)}{\langle B_\phi \rangle} = 1.6$) used as a reference throughout the Letter. The simulation involves $m = 1$ modes with n up to 54, and $m = 0$ modes with n up to 25; the aspect ratio is $R_0/a = 4$ and the magnetic boundary is ideal. Second, the Hamiltonian guiding center code ORBIT [12] is used to compute magnetic field lines or particle orbits corresponding to the reference magnetic field. This field was made more realistic by extrapolating the $m = 1$ spectrum of internal modes up to $n = 250$ with an exponential decay. Newcomb's eigenfunctions provide the radial profile of these modes.

We define the mode phases as follows. The vector potential is $A = \psi \nabla z - \chi \nabla \theta$ with the gauge condition $A_r = 0$, where (r, θ, z) are the usual cylindrical coordinates, ψ and $-\chi$ are the poloidal and toroidal flux, respectively. Then the magnetic field is of the form $B = \nabla\psi \times \nabla z - \nabla\chi \times \nabla\theta$. With these notations an (m, n) mode corresponds to a component $\chi_{m,n}(\psi)\cos(k_n z + m\theta + \alpha_{m,n})$ in χ, where $k_n = -n/R_0$, and $\alpha_{m,n}$ is the mode phase.

To describe the magnetic field line structure in the MH state, we perform two gedanken experiments. In the first one we set to zero all $m = 1$ modes, but keep all the $m = 0$ ones in the ORBIT calculation. Then, $m = 0$ modes, resonating at the reversal, form a chain of islands which does not develop chaos, since the magnetic structure is symmetrical in θ, leading to conserved magnetic flux surfaces. This is shown in Fig. 1(a): the chain of islands, with their respective O and X points, stretches continuously, throughout the toroidal direction (the picture is an equatorial cut of a torus, with the toroidal angle and the minor radius in the x and y directions, respectively; $\phi = z/R_0$). All of the modes have the same phase ($\alpha_{0,n} = 0$, $\forall n$).

In the second gedanken experiment we keep the $m = 1$ components and set to zero all $m = 0$ modes in the ORBIT calculation. Then we get the less obvious result that $m = 1$ modes alone do form an $m = 0$ chain of islands too, as shown in Fig. 1(b), which draws its origin from the beating of $m = 1$ modes, as shown below in the Hamiltonian formalism. The island chain is not continuous in the toroidal angle, but it is interrupted at $\phi = 0$. This is due to *phase locking*: all of the $m = 1$ modes tend to lock-in phase in the MH SPECYL simulations ($\alpha_{1,n} = 0$ $\forall n$). This is the numerical analogue of the possibly rotating MH bulging of the RFP plasma known as "large helical deformation" (LHD), or "slinky" [13].

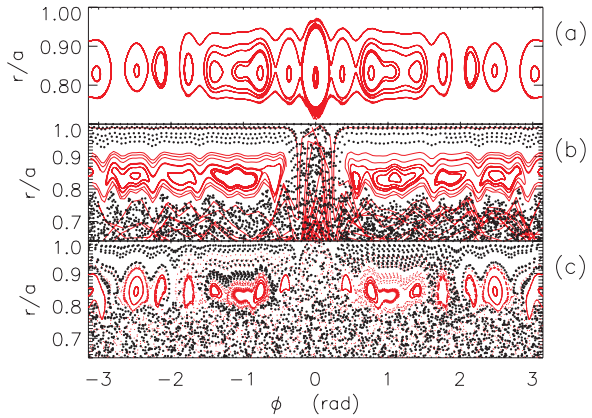

FIG. 1 (color online). Poincaré plot of magnetic field lines in the (r, ϕ) plane (a) $m = 0$ modes only, (b) $m = 1$ modes without $m = 0$ modes, (c) $m = 0$ and $m = 1$ modes together.

Figure 1(c) displays the $q = 0$ island chain due to the cooperative effect of the above $m = 0$ modes and $m = 1$ beating. In such a system the LHD is still present and now weakly chaotic regions near the X points are present.

To understand transport in this MH state, we simulated the behavior of ions with bulk energy (250 eV), interacting with the background through suitable classical and pitch-angle scattering operators. The dimensionless collision frequency related to this interaction is $\nu\tau_{\mathrm{tor}} = 1.5$ where τ_{tor} is the (toroidal) transit time and ν refers to the collisionality estimated in the RFX device [1]. The reference magnetic configuration is the case shown in Fig. 1(c), with locked $m = 0$ and $m = 1$ modes ($\alpha_{0,n} = \alpha_{1,n} = 0$), but, to single out the contribution to transport due to the LHD, and to better study the weakly chaotic region near the X points, we also consider a case where the phases of the $m = 0$ and $m = 1$ modes are randomized. In such a system the LHD is no longer present, but the weakly chaotic regions near the X points are still observed. The Poincaré plot related to this case is shown in Fig. 2(a).

We define the loss time of test particles deposited in the core as the time spent by 50% of uniformly toroidally distributed particles, plus one, to travel from the deposition radius ($r_{\mathrm{dep}} = 0.2 \times a$) to a prescribed radius r_{col}, where they are collected. The profiles of $\tau_{\mathrm{loss}}(r_{\mathrm{col}})$ for random and locked phases are rather flat in the core, and display a steep gradient near the reversal surface [Fig. 2(b)], indicating the presence of a transport barrier. We also notice that the slowing down of particle transport starts at a value of r/a smaller by $\simeq 10\%$ than the reversal radius of the mean axial field ($r/a \simeq 0.84$) indicated by the dashed line in Fig. 2(b) and by the island O points in 2(a). This shows that the transport barrier occurs before the reversal surface, as could be expected due to the finite island width. In addition, if we compare the τ_{loss} profiles with random and locked phases, we see that in the random case the loss time is larger.

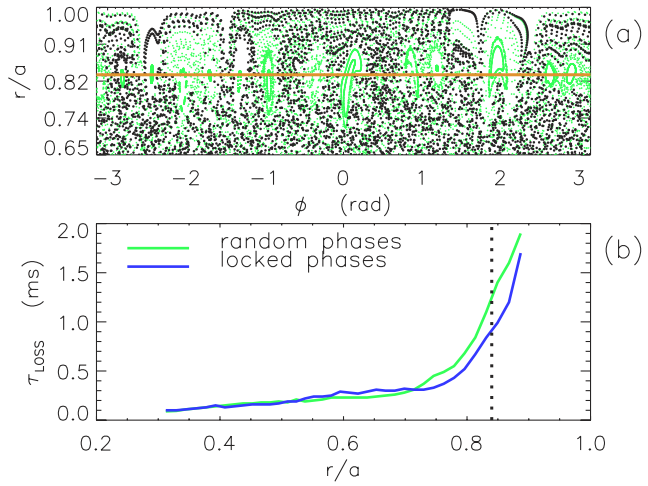

FIG. 2 (color online). (a) Poincaré plot with random phases for the $m = 0, 1$ modes; (b) radial profile of loss times τ_{loss} in two conditions (green=random, blue=locked phases). The dashed line in (b) corresponds to the reversal surface [orange line in (a)].

To understand these differences, and to visualize the different behaviors of particle motion across the structure with or without the LHD, we show, in Fig. 3, how particles deposited at $r/a = 0.7$ are transported radially when time increases (top to bottom of the figure). The left part corresponds to random phases, while the right one corresponds to phase locking. Radial transport turns out to be localized close to $\phi = 0$ in the latter case, with stronger particle oscillations toward low r/a's (which means a strong connection of edge and core plasmas). This is consistent with the fact that in Fig. 2(b) the difference between random and locked cases is not confined in the edge, but it is already visible at $r/a \approx 0.72$. An experimental indication of this edge-core connection is the occurrence of a thermal crash of high current MH discharges in concomitance with the cooling of the plasma in the LHD region in RFX [14].

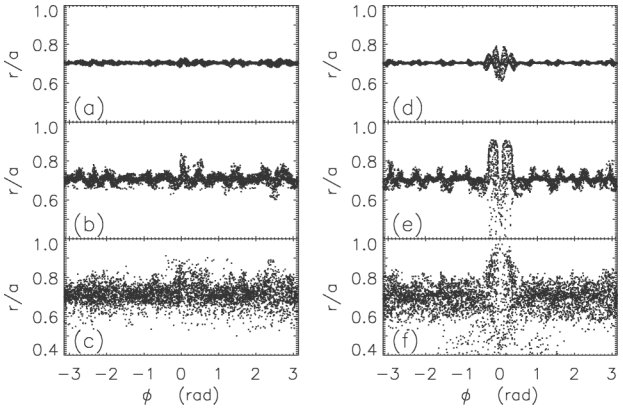

FIG. 3. Diffusion plots of test particles: particles are deposited at $r/a = 0.7$, and allowed for diffusing in the plasma (top to bottom corresponds to increasing time steps). (a)–(c) phases are random; (d)–(f) phases are locked.

As shown in the discussion of Fig. 1, the $q = 0$ islands survive in the presence of a realistic MH spectrum. Different decay laws in n have been checked, without changing our conclusions. Since experiments, such as TPE-RX [4] and MST [15], show that the increase of $m = 0$ mode amplitude is detrimental for confinement, we performed a parametric study of the evolution of loss times with the $m = 0$ amplitude. First, in order to compare our result to the experimental ones, we scaled down the amplitude of the numerical spectrum of modes to reach the experimental order of magnitude for a Lundquist number $S = 10^6$, as shown in [16]. By this procedure a new reference spectrum was obtained scaled down by 0.4 (which, in particular, means: $\tilde{b}_{m=0}/B_\theta(a) \approx 0.4\%$). Figure 4(a) displays a blowup of the Poincaré map referring to this new reference spectrum. Then, increasing by a factor of 5 the $m = 0$ spectrum, chaos is stronger, but $q = 0$ islands are still present [Fig. 4(b)]. Finally, Fig. 4(c) displays $\tau_{\rm loss}(0.98a)$ as a function of $\tilde{b}_{m=0}/B_\theta(a)$. $\tau_{\rm loss}$ decreases by almost a factor of 3 in the considered range of $\tilde{b}_{m=0}/B_\theta(a)$, consistently with the increase of chaos displayed in the maps. By defining an empirical diffusion coefficient as $\langle D\rangle = (r_{\rm col} - r_{\rm dep})^2/2\tau_{\rm loss}(r_{\rm col})$, we find an almost linear growth with $\tilde{b}_{m=0}/B_\theta(a)$, in agreement with experiments [4].

In order to understand the above numerical results, we now introduce the classical description of magnetic field lines as orbits of a Hamiltonian system [17], as it enables the direct application of concepts and tools of Hamiltonian chaos to the magnetic field structure. As B_θ does not reverse in the RFP, ψ is single valued and monotonic with respect to r. Therefore ψ, z, and θ may be taken as independent variables. It is easily checked from the previous expression for B that $\chi(\psi, z, \theta)$ is the requested

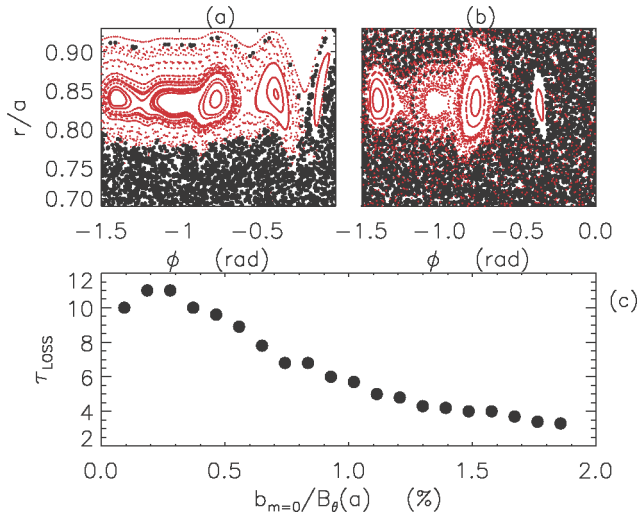

FIG. 4 (color online). (a) Poincaré map obtained with mode amplitudes scaled down to experimental values; (b) same map, obtained by multiplying the $m = 0$ amplitude by 5; (c) $\tau_{\rm loss}$ evaluated at the edge, as a function of the normalized $m = 0$ amplitude.

Hamiltonian, where ψ and z are the conjugate variables, and θ plays the role of time. The relation $\psi = \psi(r)$ makes easy the translation of the puncture plots displayed in this Letter into Poincaré plots in conjugate variables. The case where there are only $m = 0$ modes corresponds to a Hamiltonian $\chi_{m=0}$ which is θ independent and thus integrable. However, this Hamiltonian as a function of z may have several extrema. As for the motion of a particle in a potential with several extrema, this brings in phase space an island structure corresponding to nested 8-shaped separatrices. These features are visible in Fig. 1(a).

The Hamiltonian corresponding to Fig. 1(b) is $\chi_{m=1}(\psi, z, \theta) = \chi_0(\psi) + \epsilon\sum_n \chi_{1,n}(\psi)\cos(\phi_n)$ where n runs over the set of $m = 1$ modes of interest and where $\phi_n = k_n z + \theta + \alpha_n$. It is the sum of an axis-symmetric part and of a series of $m = 1$ resonant terms (''resonances'') of order epsilon. Consider the canonical transformation T from (ψ, z) to (Ψ, Z) defined by the generating function $G(\Psi, z, \theta) = \Psi z - \epsilon\sum_n \chi_{1,n}(\Psi)\sin(\phi_n)/[k_n q(\Psi) + 1]$, where $q(\psi) = \partial\chi_0(\psi)/\partial\psi$. It yields $Z = \partial G/\partial\Psi$ and $\psi = \partial G/\partial z = F(\Psi, z, \theta)$, where $F(\Psi, z, \theta) = \Psi - \epsilon\sum_n k_n\chi_{1,n}(\Psi)\cos(\phi_n)/[k_n q(\Psi) + 1]$; then the new Hamiltonian is $\chi'_{m=1} = \chi_{m=1} - \partial G/\partial\theta$. Transformation T suppresses the resonances of $\chi_{m=1}$ to order ϵ. Therefore, in Hamiltonian $\chi'_{m=1}$, resonances are of order ϵ^2 only, which means that Ψ is closer to be a constant along field lines. The ϵ^2 terms correspond to the beating between the resonant terms of $\chi_{m=1}$, and are therefore either of the $m = 0$ or of the $m = 2$ type. The $m = 0$ terms in $\chi'_{m=1}$ reveal the existence of a series of $m = 0$ islands in the (Ψ, Z) dynamics that translate into $m = 0$ islands in the (ψ, z) dynamics too.

Since $\chi'_{m=1}$ is angle independent at order ϵ, setting $\Psi =$ const in $\psi = F(\Psi, z, \theta)$ yields an approximation, correct to order ϵ, of the shape of the flux surfaces when they exist. If there is phase locking of the various $m = 1$ Fourier terms in $\chi_{m=1}$, this translates into a graph of F as a function of z with a zigzag next to $z = 0$. So is the graph of $\psi(z)$, and, consequently, that of $r(z)$. Since F has only a finite number of Fourier components, its graph displays a series of rapid oscillations both in the positive and negative ψ directions (the celebrated Gibbs phenomenon). In fact the zigzag applies to the chaotic sea as well, which explains how this sea intrudes toward large r's at $\phi = 0$. As a consequence, radial transport results from the combination of a coherent zigzag and of chaotic transport which brings a topological connection between the core and the edge. This is visible in Figs. 3(d)–3(f) also. In Fig. 3(f) the zigzag provides particles backscattered up to $r/a \approx 0.4$. In Figs. 3(a)–3(c), since the α_n's are random, F is no longer Dirac-like as a function of z, which decreases transport, but the small denominators in the transformed Hamiltonian still bring in chaos.

The generating function G has denominators $D_n \equiv k_n q(\Psi) + 1$ which vanish for $\Psi = \psi_n$ where ψ_n is the

resonant value of ψ corresponding to mode $(1, n)$. As a result in the expression for $\chi'_{m=1}$, products of these denominators are present. These denominators are small for Ψ close to the ψ_n's, which brings the breakup of Kolmogorov-Arnold-Moser tori (magnetic surfaces) and triggers chaos in the region where the $m = 1$ modes are resonant. Let ψ^* be the resonant value of ψ corresponding to $(0, n)$ modes defined by $q(\psi^*) = 0$. For Ψ close to ψ^*, the D_n's are large, which brings little chaos there.

The Hamiltonian corresponding to Fig. 1(c) is $\chi_{m=0,1}$, which is the sum of $\chi_{m=0}$ and of the resonant part of $\chi_{m=1}$. If we perform again the change of coordinates defined by G, we find a Hamiltonian $\chi'_{m=0,1}$ where the $m = 0$ contribution comes from both the $m = 0$ modes of $\chi_{m=0}$ and from the beating of the $m = 1$ modes of $\chi_{m=1}$ already present in $\chi'_{m=1}$. As a result, the island structure in Fig. 1(c) is the result of a cooperative action of the $m = 0$ and $m = 1$ terms of $\chi_{m=0,1}$. The zigzag of the chaotic sea can be understood as above. If the $m = 0$ modes are chosen so as to cancel exactly the $m = 0$ contribution of the beating of the $m = 1$ modes in $\chi'_{m=0,1}$, no $m = 0$ contribution is present in this Hamiltonian, which decreases chaos at reversal. This latter result implies that the presence of $m = 0$ resonances is not always negative, in contrast to what occurs for the experimental phase relation of the MHD modes as shown in Fig. 4. This indicates a possible way of controlling the $q = 0$ barrier. It consists of trying to obtain a no-resonance, no-island condition, by reducing the overall $m = 0$ resonance amplitude, with a local compensation of both $m = 0$ modes and the $m = 0$ terms of the $m = 1$ beating present in $\chi'_{m=0,1}$. This operation will be attempted in RFX by means of the new toroidal coil system [18]. A still open issue is how the plasma is going to react, MHD-wise, to the externally applied field. This could complement previous attempts to diminish chaos, either by exploiting the existence of a spontaneous, helically symmetric state called quasisingle helicity (QSH) [19], or by applying a time-varying electric or magnetic field at the edge [15,20,21].

We can define a canonical transformation suppressing all resonances of $\chi_{m=0,1}$ to order ϵ by completing G with new terms tailored for the resonant terms of $\chi_{m=0}$. Because of the $m = 0$ modes, the transformed Hamiltonian has resonant terms with denominators involving powers of $q(\Psi)$. These denominators are now small for Ψ close to ψ^*, which explains why chaos is stronger in the reversal region in Fig. 1(c) than in Fig. 1(b). In Fig. 1(c), as usual, chaos develops from the 8-shaped separatrices of the $m = 0$ resonance to form chaotic layers which are now thick enough to be visible. However in such thicker layers the motion must still come close to the X points which are perturbed versions of those of the $m = 0$ island defined by $\chi_{m=0}$ (these points are structurally stable). Linear theory tells that a close encounter with an X point is a slow process, which explains why chaotic transport is shown in Fig. 2(b) to be slowed down in the island domain. This discussion sheds light on the role of toroidicity, which introduces n sidebands in the $m = 0$ spectrum [22]. These translate in an additional $\chi^{\text{tor}}_{m=0}$ term, with amplitudes $\chi^{\text{tor}}_{0,n}(\psi)$ decaying with n like the $m = 1$'s. A magnetic reconstruction of RFX ($R_0/a = 4$) has shown a change of the islands' shape, and an increase of chaos (smaller τ_{loss}), but in a way that the cylindrical picture still holds.

In conclusion, this Letter shows the existence of a transport barrier in the reversal region of the MH state. Chaos in this region might be minimized by applying an $m = 0$ perturbation related to a vanishing island amplitude. This latter condition also corresponds to an axis- or helical-symmetric RFP, which remain the ideal chaotic-transport-free configurations [19,20].

The authors wish to thank S. Ortolani, P. Zanca and D. Terranova. This work was supported by the European Communities under the contract of Association between EURATOM/ENEA.

[1] A. Intravaia *et al.*, Phys. Rev. Lett. **83**, 5499 (1999).
[2] D. Gregoratto *et al.*, Nucl. Fusion **38**, 1199 (1998).
[3] T. M. Biewer *et al.*, Phys. Rev. Lett. **91**, 045004 (2003).
[4] A. Canton *et al.*, Plasma Phys. Controlled Fusion **46**, 23 (2004).
[5] L. Marrelli *et al.*, J. Nucl. Mater. **266–269**, 877 (1999).
[6] A. Cravotta *et al.*, Phys. Plasmas **10**, 4737 (2003).
[7] L. Carraro *et al.*, J. Nucl. Mater. **313–316**, 976 (2003).
[8] P. Zanca and S. Martini, Plasma Phys. Controlled Fusion **43**, 121 (2001).
[9] F. D'Angelo and R. Paccagnella, Phys. Plasmas **3**, 2353 (1996).
[10] M. Valisa *et al.*, J. Nucl. Mater. **241–243**, 988 (1997).
[11] S. Cappello and D. Biskamp, Nucl. Fusion **36**, 571 (1996).
[12] R. B. White and M. S. Chance, Phys. Fluids **27**, 2455 (1984).
[13] T. Tamano *et al.*, Phys. Rev. Lett. **59**, 1444 (1987).
[14] M. Valisa *et al.*, in *20th IAEA Conf., Vilamoura, Portugal* (IAEA, Vienna, 2004).
[15] B. E. Chapman *et al.*, Phys. Rev. Lett. **87**, 205001 (2001).
[16] D. Terranova *et al.*, Plasma Phys. Controlled Fusion **42**, 843 (2000).
[17] A. H. Boozer, Phys. Fluids **26**, 1288 (1983); F. Doveil, Journal de Physique **45**, 703 (1984).
[18] V. Toigo *et al.*, in *20th Symposium on Fusion Eng.* (IEEE/NPSS, San Diego, USA, 2003), p. 371.
[19] P. Martin *et al.*, Nucl. Fusion **43**, 1855 (2003).
[20] F. Ebrahimi and S. C. Prager, Phys. Plasmas **11**, 2014 (2004).
[21] J. W. Long *et al.*, in *11th EPS Conference, Aachen, Germany* (European Physical Society, Petit Lancy, 1983), Vol. 7D, Part I, p. 159.
[22] P. Zanca and D. Terranova, Plasma Phys. Controlled Fusion **46**, 1115 (2004).